Toward Phase Stability: Dion–Jacobson Layered Perovskite for Solar Cells

Peng Huang [a], Samrana Kazim [a,b], Mingkui Wang [c], and Shahzada Ahmad [a,b*]

[a] BCMaterials, Basque Center for Materials, Applications and Nanostructures, Martina Casiano, UPV/EHU Science Park, 48940 Leioa, Spain

Tel: +34 946128811 Email: shahzada.ahmad@bcmaterials.net

[b] IKERBASQUE, Basque Foundation for Science, Bilbao, 48013, Spain

[c] Wuhan National Laboratory for Optoelectronics, School of Optoelectronic Science and Engineering, Huazhong University of Science and Technology, Wuhan, 430074, China

Abstract

Three-dimensional halide based perovskites has emerged as promising semiconducting light harvester for thin-film solar cells fabrication, however, its intrinsic instability under humidity restricts their potential commercialization. To address such challenges, the development of low-dimensional Dion-Jacobson (DJ) phase / layered perovskites have recently gained substantial attention due to their intriguing environmental stability and competitive power conversion efficiency. In this review, we have screened and focused our investigation on the DJ phase in layered perovskite for solar cell fabrication, especially elucidation on the active role played by organic spacer cation for active layer. We also discuss the possible strategies that can be employed to further push the performance of DJ perovskite solar cells.

1. Introduction

Perovskite solar cells (PSCs) have witnessed an unprecedented investigative development as potential photovoltaic (PV) materials since the first report on organo halide perovskite for dye-sensitized solar cell by Miyasaka in 2009.[1–8] The unparalleled

advancement of PSCs is ascribed due to the opto-electrical properties of halide perovskite, such as high absorption coefficient and tunable direct bandgap,[9–11] long charge diffusion length and excellent carrier mobility[12–16] together with the possibility of being deposited by low-cost solution-processable route.[17–22] Recently, certified power conversion efficiency (PCE) of 25.2% in the lab has been reported by KRICT and MIT,[23] which is the highest PCE for any thin-film PV technology and fulfill the cost to performance ratio requirements for renewable power generation. However, two major challenges such as the issue of toxicity of lead (Pb) and long-term intrinsic instability of PSCs may limit their future commercialization.[24–28] To resolve the issue of lead toxicity, other less toxic metal such as tin (Sn^{2+}), germanium (Ge^{2+}), antimony (Sb^{3+}), silver (Ag^{+}) and copper (Cu^{2+}) can be exploited to replace Pb completely or partially.[29]

Different strategies have been adopted to enhance the stability of PSC devices, including doping and compositional engineering of perovskites,[30–37] interface modification,[2,38–41] developing innovative electron and hole transporting materials [42–47] and new encapsulation techniques,[48–50], *etc.* Recently, by reducing the dimensionality of perovskites from 3-dimensional (3D) to lower dimensionality was found to be an effective approach for enhancing the stability.[51–54] Low dimensional/layered perovskites are also referred in literature as 2-dimensional perovskites and their extraordinary stability stems from their low-ion migration and water-resistant nature due to their sandwich structure. Among the layered halide perovskites, (100) oriented perovskites are the most common, which is formed by cutting along the (100) plane in 3-D perovskite and among them, Ruddlesden−Popper (RP) phase containing two mono cation and Dion−Jacobson (DJ) phase containing one dication were the recently investigated for PV applications.

In 2014, Karunadasa and co-workers were the first to report layered RP phase $(PEA)_2(MA)_2Pb_3I_{10}$-based PSCs, which exhibited excellent resistance to moisture and

PCE up to 4.73%.[55] Since then, the PCE of layered RP PSCs have risen significantly up to 18.2% .[55–59] Recently, DJ phase layered perovskites have evolved as promising materials for PV application and a steep rise from 7.32% to 17.9% in PCE was witnessed within a year (**Figure 1**).[53,60–64] These significant developments demonstrate the tremendous potential of the DJ phase perovskites for their application as semiconducting active layers aiming to fabricate efficient and long-term stable PSCs.

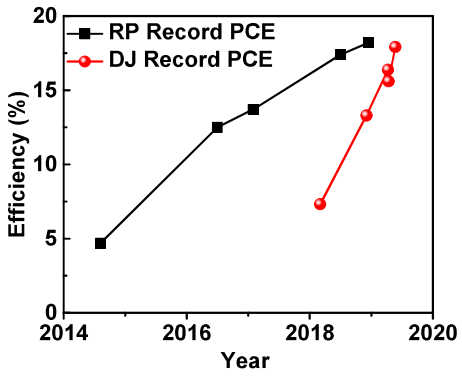

Figure 1. Evolution of the record PCE for layered RP, DJ PSCs.

Here, we will focus on chemical modification of organic (spacer) group and its bearing on structural, opto-electrical and device performance of DJ based perovskite and thereof its utilization for PV application. We have also outline the challenges and possible strategies to overcome the bottleneck in DJ based perovskite to further optimize the performance.

2. Structure and Properties of 2-dimensional / layered Perovskites

The typical 3-dimensional halide perovskite has the formula of ABX_3, where A is a monovalent cation of methyl ammonium (MA^+), formamidinium (FA^+), cesium (Cs^+) or rubidium (Rb^+), B is a divalent metal cation (Pb^{2+} or Sn^{2+}, *etc.*) and X is a halide anion (I^-, Br^- or Cl^-). This structure is comprised of the corner shared $[BX_6]^{4-}$ octahedral with

A^+ cation which occupies the voids as shown in **Figure 2a**. Layered perovskites are conceptually achieved by cutting along the crystallographic planes <100>, <110> or <111> of 3D perovskite structure, which results in the formation of three different types of layered perovskite, namely the <100>, <110> or <111>-oriented layered perovskites.[65] Among these three kinds of perovskites, the <100>-oriented layered perovskites are so far the commonly employed as compared to others (Figure 2b). The <100>-oriented perovskites can be categorized as layered RP and DJ perovskites, respectively (the structure of different phase layered perovskites with n = 3 as examples showed in Figure 2c). From a crystallographic point of view, layered perovskites were derived from oxides perovskite, inorganic semiconductor layers in hybrid organic-inorganic RP layered perovskites are offset by per unit cell, showing a (1/2, 1/2) in-plane displacement along the *ab*-plane. As a result, the inorganic layers enforced in a staggered configuration. On the other hand, the inorganic layers in the DJ phase perovskites do not exhibit any shift with (0, 0) in-plane (or a minor displacement) and are stacked perfectly on top of each other resulting in an eclipsed like stacking arrangement, which is slightly different with DJ perovskites as compared to oxides perovskite exhibiting relative (1/2, 0) shift or no shift (0, 0) at all.[53,66,67] The layered RP and DJ phase perovskites can be expressed as $A'_2A_{n-1}B_nX_{3n+1}$ and $A''A_{n-1}B_nX_{3n+1}$, respectively, where, A′ and A″ are monovalent (+1) and divalent (+2) aromatic or aliphatic alkyl ammonium spacer cations, respectively, while A is organic cation, X is a halide anion, B is a divalent metal.

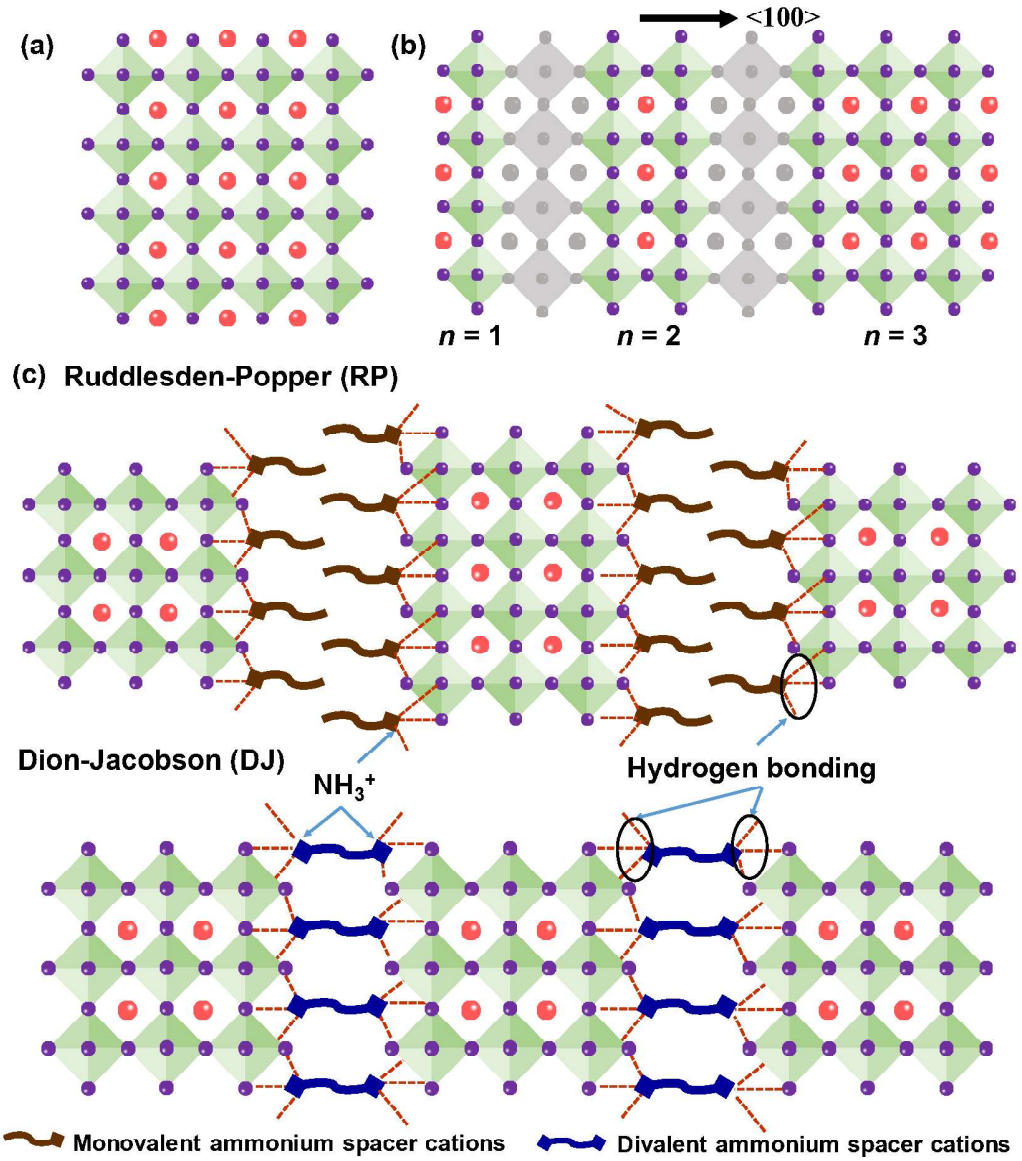

Figure 2. (a) Crystal structure of a 3D perovskite, (b) The structure derivation of layered perovskite with spacer cations cutting the 3D perovskite from <100> planes and (c) Crystal structures of RP and DJ phase layered perovskites (n=3).

The value of "*n*" is defined as the number of perovskite slabs ($[BX_6]^{4-}$ octahedral sheets sandwiched between two layers of spacer cations), which can be experimentally achieved by judiciously modulating the stoichiometry of initial precursors. *n* is a crucial factor in determining opto-electrical properties of layered perovskites, influencing the

bandgap and consequently its absorption as well as conductivity/mobility and stability. The value of *n* in most of the reported PSCs having >10% efficiency is over 3. However, it is difficult to obtain phase-pure perovskite with high *n* values,[68] and the results about RP and DJ phase layered perovskite can be indeed still questioned from the viewpoint of phase purity. According to the phase purity, layered perovskites for PV devices can be divided into three major categories: (i) phase-pure layered perovskites, (ii) mixed 2D/3D phase perovskites, (iii) passivating perovskite layers. All of these will be discussed in details as following:

(i) phase-pure layered perovskites: Most of the current papers about phase purity of layered perovskites focused on perovskites with low *n* values (*n* = 1, 2), which are unsuitable for PV applications, as they possesses large band gap and poor charge transportation, while further increase in the value of *n* leads to high photocurrents due to the reduction of the excitonic effect and improve charge carrier transport. Thus, the research of phase-pure perovskites with high *n* values are vital for layered perovskite aiming to PV application. However, this part of research are currently lagging behind and there are few reports dealing with the opto-electrical properties of layered perovskite with high *n* values ($n \geq 5$).[54,68–70] For example, Kanatzidis and co-workers reported about the thermodynamic stability and chemical synthetic limitations of $BA_2MA_{n-1}Pb_nI_{3n+1}$ layered RP with high phase purity (*n* = 1-7). The authors found that it is challenging to synthesize phase-pure layered RP perovskite with n > 7 due to their thermodynamically instability. The enthalpy of formation (ΔH_f) are negative for compounds with *n* = 1-5 but positive for the compounds with a higher *n* (*n* = 6 and 7). The ΔH_f should be negative to allow a negative Gibbs free energy (ΔG) to favor the reaction (**Figure 3a**). This suggest that layer RP perovskite with "*n* = 9" according to the stoichiometry of the precursor can't form in pure form and formed in a mixture of $MAPbI_3$ with higher-*n* values RP phase

perovskite.[68] Later, crystallographically characterized DJ phase perovskite with $n = 7$ was reported. The DJ phase perovskites have a smaller degree of distortion in the crystal structure than RP phase counterparts. Which in turn allow DJ perovskites to have improved opto-electrical properties (lower energy absorption edge and photoluminescence emission) suitable for PV applications.[70]

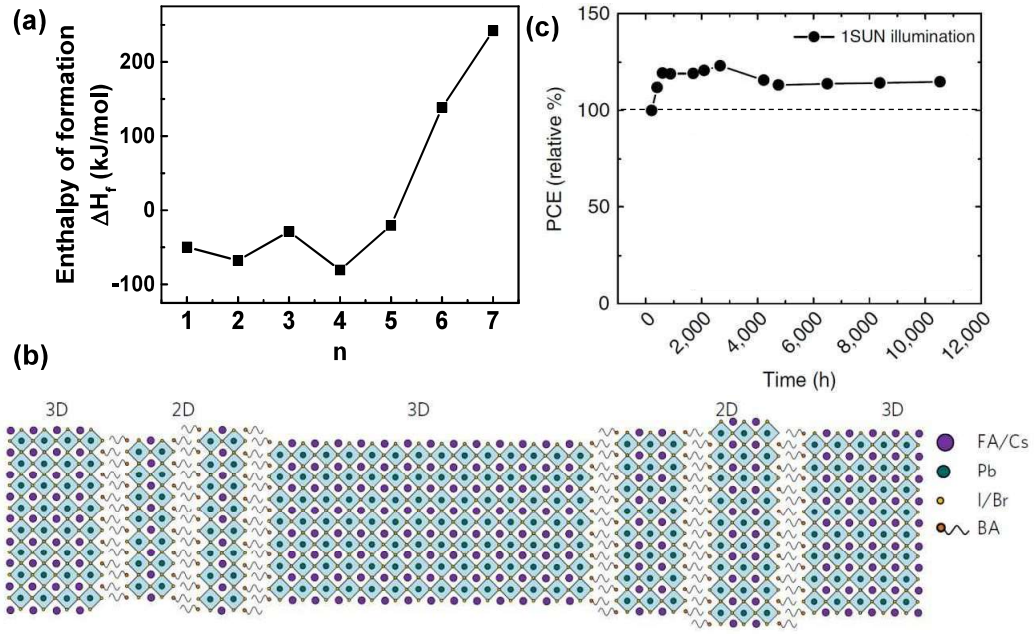

Figure 3. (a) Enthalpy of formation of the $(BA)_2(MA)_{n-1}Pb_nI_{3n+1}$ series as a function of the perovskite layer thickness (n). Data obtained from reference 68. (b) Schematic illustration of the proposed mixed layered (2D) /3D phase perovskite film structure. (CB_{3D}/VB_{3D}: conduction band/valence band of 3D perovskite, CB_{2D}/VB_{2D}: conduction band/valence band of 2-dimensional perovskite), reprinted from reference 72. Copyright 2017 Springer Nature, (c) Typical module stability test under 1 sun AM 1.5 G conditions at a stabilized temperature of 55° and at short circuit conditions. Reprinted with permission from ref 38. Copyright 2018 NPG Publishing Group.

(ii) Mixed layered (2D) / 3D phase perovskites. Mixed 2D/3D phase perovskites were obtained by introducing spacer cations with relatively low concentration in 3D perovskite films, suggesting that the typical value of *n* in corresponding perovskite will be greater than 7.[71] The *n* value in the mixed layered (2D) /3D phase perovskites can be called as effective "*n* value", which can reach up to "60" or higher in this structure. This structure is different from the phase-pure layered perovskite but plays a vital role in optimizing parameters, especially V_{oc} and improving stability of the device. For example, Snaith and co-workers incorporated a layered perovskite with a wide bandgap 3D perovskite in between grains. When photo charge carriers transport to the grain boundary of 3D perovskite, they are blocked by the layered perovskites, it remains in the 3D perovskite and propagate in the grain without getting trapped or recombination at grain boundaries defects (Figure 3b).[72] Sargent *et.al* elucidated the reason of mixed layered (2D) / 3D phase perovskite with high stability compared to 3D counterparts via theoretical and experimental investigations. The very low formation energy of 3D perovskites leads to their low stability, while mixed layered (2D) / 3D phase perovskite possesses much higher formation energies owing to significant van der Waals forces.[58] The PSCs with mixed layered (2D) / 3D $(HOOC(CH_2)_4NH_3)_2PbI_4/CH_3NH_3PbI_3$-based phase perovskite kept initial efficiency without any loss in performance measured under standard conditions and in the presence of oxygen and moisture (Figure 3c).[38]

(iii) Passivating perovskite layers. Employing a very thin-layered perovskite as a capping layer atop of 3D perovskite films is alternative usage to layered perovskite. In this case, the definition of *n* values and phase purity of layered perovskite is not straightforward. The capping layers were presented to play as a passivating layer to decrease both the cation and anion defects on the surface via hydrogen bonding or ionic bonding, which cause non-radiative recombination to affect the device performance.

Besides, the 2-dimensional perovskite layer act as encapsulating hydrophobic layers to improve the stability of the devices. For example, Bawendi and co-workers prepared a layered (2D) perovskites containing long linear alkane amine radicals atop of 3D perovskite. Thus, the 3D perovskite modified by layered (2D) presented the hydrophobic surface and the corresponding device showed improved efficiency and stability.[73]

Layered/low dimensional perovskites exhibit distinctive properties due to their unique crystal structure. Firstly, layered perovskites present a strong exciton binding energy (E_b) related to quantum and dielectric confinement effects. It should be noted that the quantum and dielectric confinement effects in layered hybrid perovskite have been systematically reviewed by Even and co-workers[74] and in brief we described here. The semiconducting inorganic layers composed of *n*-layers perovskite slabs act as "wells" and the organic dielectric spacer cation layers serve as "barriers" in type-I quantum well of layered perovskites (**Figure 4a**).[75] The quantum well arises from a wider bandgap of organic layers compared to inorganic layers. A gradual rise of quantum well as the *n* values increases leads to a blue-shift of exciton absorption onset and sharp emission of layered perovskites in a wide range of wavelength (Figure 4b & 4c).[76] The dielectric confinement is caused by the mismatch of dielectric constants between inorganic layers (¨wells¨) and organic spacer cations (¨barriers¨). Theoretically, the binding energy (E_b) of layered perovskites can be calculated by the following equation: $E_b = 4(\frac{\varepsilon_w}{\varepsilon_b})^2 E_b^{3D}$, where ε_w and ε_b are the dielectric constants of the ¨wells¨ and ¨barriers¨, respectively. E_b^{3D} represents the exciton binding energy of the corresponding 3D perovskite.[77] Expectedly, the dielectric constant of organic spacer cations (ε_b) is lower than that of inorganic layers (ε_w). According to the equation, the dielectric confinement can be tuned by varying the composition of inorganic and organic layers. Molecular design approach taking into account both the structural tolerance, growth kinetics and doping is effective way to

prepare excellent layered perovskite films with low E_b.[57] For example, Karunadasa and co-workers reported decreasing exciton binding energy via post-synthetic I_2 molecule intercalation. The intercalants afford organic layers that are more polarizable than the perovskite layers, and reduces the exciton confinement in the inorganic layers and decrease the exciton binding energy in $(IC_6H_{12}NH_3)_2[PbI_4]$ perovskite.[78]

Recently, a general empirical scaling law to calculate the exciton binding energy of layered perovskites based on Keldysh theory was developed by Mohite and co-workers, which makes it easier for researchers to know the confinement effects and exciton binding energy of the layered perovskites.[79] The equation is as follows: $E_{b,1s} = \frac{E_0}{(1+\frac{\alpha-3}{2})^2}$ with $\alpha = 3 - \gamma e^{-L_w/2a_0}$, where E_0 (16 meV) and a_0 (=4.6) are the 3D Rydberg energy and Bohr radius of 3D perovskites,[80] respectively, and L_w is the physical width of the quantum well for an infinite quantum well potential barrier.[81] The empirical correction factor γ (=1.76) was used to correct the exciton binding energy effected by the synergistic effect of quantum and dielectric confinement instead of quantum confinement effect.[82] Figure 4d & 4e present a comparison between experimentally obtained dimensionality coefficient α and binding energy E_b with theoretical values. The law for E_b predicts free carrier like behaviour for layered RP phase perovskites with n value larger than 20.

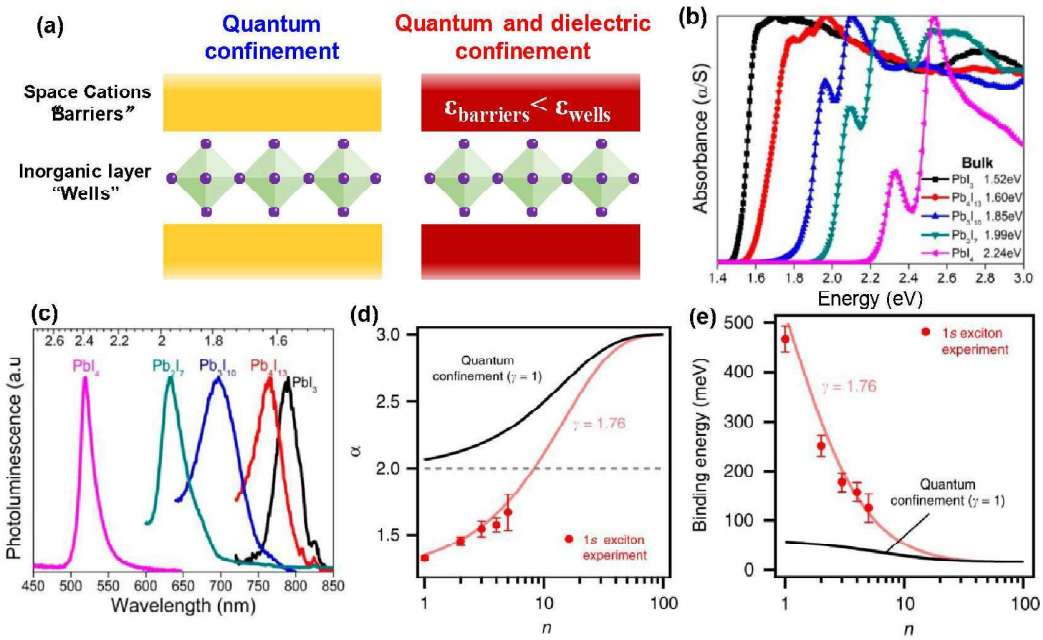

Figure 4. (a) Layered perovskite with confinement effects, (b) Optical band gaps of bulk and (c) PL spectra of spin-coated thin film of 3D $MAPbI_3$ expressed as PbI_3 and $(BA)_2MA_{n-1}Pb_nI_{3n+1}$ compounds shown as PbI_4 (n = 1), Pb_2I_7 (n = 2), Pb_3I_{10} (n = 3), Pb_4I_{13} (n = 4), respectively. Reproduced from reference 76. Copyright 2015 American Chemical Socicty. (d) Thc dimcnsionality cocfficicnt α dcrivcd from $\alpha = 3 - \gamma e^{-L_w/2a_0}$, (c) Comparison between experimentally obtained binding energies with theoretical values. Reprinted with permission from reference 82. Copyright 2018 NPG Publishing Group.

Further, layered perovskites possess distinct opto-electrical properties, which can be controlled by the components of perovskite slabs and kinds of organic spacer cations used. Cation size, shape (steric effect), charge (electrostatic attraction), and the position of the functional groups (II-bonding and dispersion forces) of spacer cations determine the unique properties of layered perovskites. For example, the bandgap of layered perovskites can be altered by introducing different spacer cations due to their influence on the *B-X-B* angle.[53, 83, 84] Up to now, most commonly monovalent ammonium spacer cations such as

phenylethylammonium (PEA)[58,85] and butylammonium (BA)[51,86] have been reported for layered RP perovskites. Divalent ammonium spacer cations includes 3-(aminomethyl)piperidinium (3AMP), 4-(aminomethyl)piperidinium (4AMP), 3-(aminomethyl)pyridinium (3AMPY) and 4-(aminomethyl)pyridinium (4AMPY), 1,4-phenylenedimethanammonium (PDMA), 1,3-propane-diamine (PDA), 1,4-butanediamine (BDA), 1,5-pentamethylenediamine (PeDA), and 1,6-hexamethylenediamine (HDA), 1,8-Octanediamine (ODA) for DJ perovskites as shown in **Figure 5**.

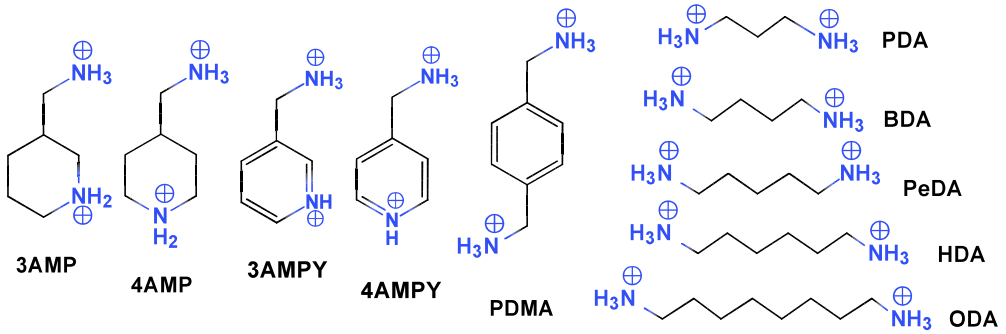

Figure 5. Chemical structure of spacer cations in DJ perovskites and used in PV application. Recently, the competitive advantages of DJ perovskites over RP counterparts were reported, such as improved stability, and higher conductivity/mobility owing to the divalent ammonium cations which combine with perovskite slabs at both sides by chemical bonding in DJ perovskite while monoamine ammonium cations interact with perovskite slabs at only one side and thus it presents a van der Waals gap in RP perovskite (Figure 2c). We direct the readers to recent excellent reviews focusing on layered RP phase in PSCs,[87–90] and here, we will highlight the recent development in layered DJ PSCs.

3. Layered DJ perovskite for PV application

Table 1 lists DJ perovskite for PSCs fabrication having different spacer cations and their impact on PV parameters. Up to now, piperidinium derivatives and their aromatic

analogs, alkyl-chain diamine and benzene dimethanammonium are the most exploited as spacer cations for DJ perovskite.

3.1 Piperidinium derivatives and their aromatic analogs

Kanatzidis *et.al* were first to report layered DJ PSCs by introducing 3AMP and 4AMP as a spacer cations.[53] PSCs with DJ perovskites (*n = 3, 4*) as light harvester were fabricated in a planar *p-i-n* solar cells architects (**Figure 6a**). Particularly, DJ PSCs with 3AMP$MA_3Pb_4I_{13}$ (*n = 4*) showed the higher PCE of 7.32% than of 4AMP$MA_3Pb_4I_{13}$ (*n = 4*) (Figure 6b). Detailed crystallographic investigation and density functional theory calculations reveal that the *B-X-B* (*Pb-I-Pb*) bond angles of 3AMP$MA_3Pb_4I_{13}$ are larger than that of 4AMP$MA_3Pb_4I_{13}$ (the *Pb-I-Pb* bond angles were classified into two categories, the axial one along the longest crystallographic axis and the equatorial one along the inorganic plane). The larger the average axial and equatorial *Pb-I-Pb* bond angle (c.a. to 180°), the more the Pb s and I p orbitals overlap (Figure 6c).[91–93] The strong antibonding interaction will push the valence band maximum, resulting in a reduced bandgap for 3AMP-based perovskite than of 4AMP-based counterparts, which led the 3AMP-based device with higher efficiency compared to 4AMP-based devices. Validating the structure property co-relationship between Pb-I-Pb bond angle and opto-electrical properties of layered perovskites, authors systematically investigated the effect of new spacer cations and component of A-site cation of perovskite slabs on Pb-I-Pb bond angle of crystal structure.

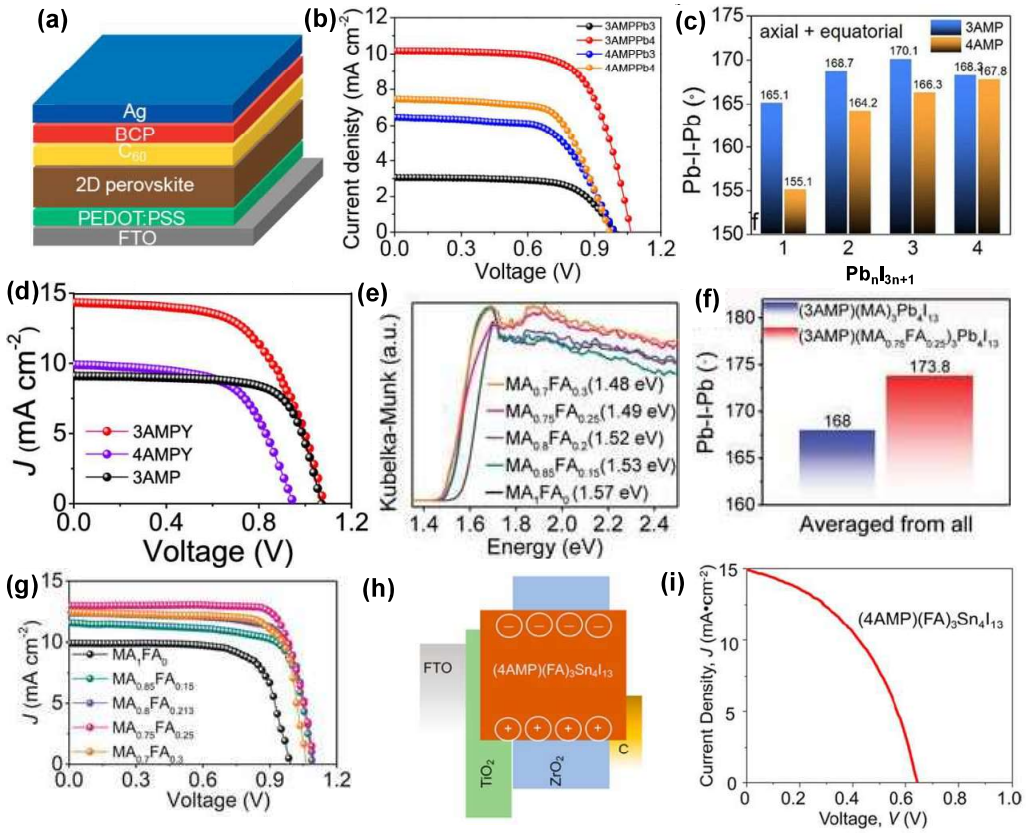

Figure 6. (a) *p-i-n* device structure adopted for DJ perovskite with 3AMP and 4AMP, (b) *J*−*V* curves of the DJ PSCs with 3AMP and 4AMP, (c) Average axial and equatorial angles for 3AMP and 4AMP. Reproduced from reference 53. Copyright 2018 American Chemical Society. (d) *J*−*V* curves of the DJ PSCs with 3AMPY (4AMPY) and 3AMP. Reproduced from reference 66. Copyright 2019 American Chemical Society. (e) Absorption and (f) angle averaged *Pb*−*I*−*Pb* for DJ perovskites with different compositions of MA^+ and FA^+, (g) *J*–*V* curves of DJ PSCs with different compositions of MA and FA. Reprinted with permission from reference 84. Copyright 2019 Wiley-VCH. (h) Energy-level diagram of *n-i-p* triple-mesoporous device structure for DJ Sn-based HTL-free PSCs and (i) *J*–*V* curve for a $(4AMP)(FA)_3Sn_4I_{13}$-based HTL-free PSC. Reproduced from reference 94. Copyright 2019 American Chemical Society.

Later, the effect of different dications such as conformation, the presence of conjugated groups, *etc.*, on the properties of the inorganic semiconducting layers in DJ perovskites by preparing the 3AMPY- and 3AMP-based films/devices (n = 4) with the same film deposition method was subject of investigation. The 3AMPY-based PSC exhibited a champion PCE of 9.20% with J_{sc} of 14.34 mA cm^{-2}, which is higher than the corresponding piperdinium analog 3AMP-based ones with PCE of 6.89% and J_{sc} of 9.11 mA cm^{-2} (Figure 6d). The improved PV performance especially the enhanced J_{sc} can be attributed to high crystallinity and vertical preferred orientation, as well as the long PL lifetime of 3AMPY-based perovskite film. More importantly, 3AMPY cation has a larger dielectric constant ($\varepsilon_b \sim 3$) than the aliphatic analogy 3AMP ($\varepsilon_b \sim 2$) due to the delocalization of π-electron system, which reduces the dielectric mismatch and resultant dielectric confinement between the inorganic well and organic barriers. Thus smaller dielectric confinement effect and low exciton binding energy is beneficial for the charge separation in the device.[66] Introducing rational spacer cations with large dielectric constant to modify the semiconducting properties of layered perovskites is a simple yet effective approach.

Further, through compositional engineering, introduction of MA^+ and FA^+ mixed cations in the perovskite slabs was found to improve the efficiency and stability of DJ PSCs based on 3AMP.[84] As depicted in Figure 6e, (3AMP)$(MA_{0.75}FA_{0.25})_3Pb_4I_{13}$ perovskite has narrower bandgap (1.48 eV) than of (3AMP)$MA_3Pb_4I_{13}$ due to its higher average Pb-I-Pb angles (173.8°) than of (AMP)$MA_3Pb_4I_{13}$ (168°) (Figure 6f). Importantly, DJ perovskite with mixed A-site cations shows preferred (011) orientation which can facilitate vertical growth on the substrate. This means minimized electrical losses and improve charge carrier transportation. This led the DJ mix-cation PSCs with planar *p-i-n*

configuration to exhibits PCE of 12.04% (Figure 6g) for champion device and with 3AMP organic spacer, mixed A-site cation DJ perovskites showed better air and light stability. These three papers systematically studied the structural properties of single-crystal, especially Pb-I-Pb bonding angle in compositional engineering layered perovskites. Arguably the combined approach of having novel spacer cations and compositional engineered of perovskite slabs can enhance the semiconducting properties and performance of corresponding PV devices.

Table 1. Summary of DJ perovskites and their solar cells performance.

[g]DJ PSCs	*n*	E_g (eV)	Device configuration	V_{oc} (V)	J_{sc} (mA cm^{-2})	**FF** (%)	**PCE** (%)	Stability
3AMP$MA_2Pb_3I_{10}$	3	1.92	FTO/PEDOT:PSS/PVK[a]/C_{60}/BCP/Ag	0.99	3.05	66.54	2.02[53]	N/A
3AMP$MA_3Pb_4I_{13}$	4	1.87	FTO/PEDOT:PSS/PVK/C_{60}/BCP/Ag	1.06	10.17	67.6	7.32[53]	N/A
3AMP$(MA_{0.75}FA_{0.25})_3Pb_4I_{13}$	4	1.48	FTO/PEDOT:PSS/PVK/C_{60}/BCP/Ag	1.09	13.69	81.04	12.04[84]	Unencapsulated devices maintained ~ 22% of their initial PCE under constant AM 1.5G illumination in ambient air (50-70% RH) for ~ 48 h
4AMP$MA_2Pb_3I_{10}$	3	1.99	FTO/PEDOT:PSS/PVK/C_{60}/BCP/Ag	0.96	6.31	60.3	3.67[b, 53]	N/A
4AMP$MA_3Pb_4I_{13}$	4	1.89	FTO/PEDOT:PSS/PVK/C_{60}/BCP/Ag	0.94	7.05	64.05	4.24 [b, 53]	N/A
4AMP$FA_3Sn_4I_{13}$	4	1.47	FTO/TiO_2/ZrO_2/PVK/C	0.64	14.9	0.443	4.22[94]	Unencapsulated devices retained 91% of their initial PCE under 1 sun illumination in N_2 atmosphere at 45 °C for 100 h.
3AMPY$MA_3Pb_4I_{13}$	4	1.87	FTO/PEDOT:PSS/PVK/C_{60}/BCP/Ag	1.08	14.34	59.58	9.20[66]	N/A
4AMPY$MA_3Pb_4I_{13}$	4	1.89	FTO/PEDOT:PSS/PVK/C_{60}/BCP/Ag	0.95	9.91	60.46	5.69[66]	N/A
PDAPbI_4	1	2.46	FTO/TiO_2/PVK/Spiro/Au	0.64	1.04	46	0.3[64]	N/A
PDA$MAPb_2I_7$	2	1.96	ITO/PEDOT:PSS/PVK/C_{60}/BCP/Ag	0.8	10.8	44.3	3.8[60]	N/A
PDA$MAPb_2I_7$	2	1.77	FTO/TiO_2/PVK/Spiro/Au	0.88	4.38	32	1.27[64]	N/A

PDA$MA_2Pb_3I_{10}$	3	-	ITO/PEDOT:PSS/PVK/C_{60}/BCP/Ag	1.04	13.5	64.4	9.0[60]	N/A
PDA$MA_2Pb_3I_{10}$	3	1.69	FTO/TiO_2/PVK/Spiro/Au	0.9	17.93	54	9.1[64]	N/A
PDA$MA_3Pb_4I_{13}$	4	1.63	ITO/PEDOT:PSS/PVK/C_{60}/BCP/Ag	0.97	18.0	74.3	13.0[60]	Encapsulated devices retained 90% at RT and 85% RH after 1,000 h. Unencapsulated devices retained 99% of their initial efficiency under continuous heating at 70 °C and 85% RH after 100 h.
PDA$MA_3Pb_4I_{13}$	4	1.63	FTO/TiO_2/PVK/Spiro/Au	0.98	19.5	69	13.3[64]	Unencapsulated device retained over 95% initial efficiency under various harsh stresses including ambient air (40%–70% RH) for 4,000 h, damp heat (85 °C and 85% RH) for 168 h, and continuous light illumination for 3,000 h.
PDA$MA_4Pb_5I_{16}$	5	-	ITO/PEDOT:PSS/PVK/PC_{60}BM/LiF/Al	0.99	19.25	74	14.16[61]	Unencapsulated devices remained ~ 28% of their initial PCE for 20 days in an ambient air with 45% RH.
BDAPbI_4	1	2.37	FTO/c-TiO_2/PVK/Spiro/Ag	0.87	2.89	43	1.082[95]	Devices retained 73.8% after 96 h.
BDAPbI_4	1	2.37	FTO/c-TiO_2/mp-TiO_2/PVK/Spiro/Ag	0.92	2.73	45	1.1[96]	N/A
BDA$MA_4Pb_5I_{16}$	5	1.6	ITO/PEDOT:PSS/PVK/PC_{60}BM/LiF/Al	1.04	20.01	78.64	16.38[61]	Unencapsulated devices remained ~ 80% of their initial PCE for 20 days in an ambient air with 45% RH.
BDA$MA_4Pb_5I_{16}$	5	-	ITO/PEDOT:PSS/PVK/PC_{60}BM/LiF/Al	1.09	22.25	73.65	17.91[62]	Unencapsulated devices remained ~ 84% of their initial PCE in an ambient air with ~ 60% RH for 1,182 h.
PeDA$MA_4Pb_5I_{16}$	5	1.65	ITO/PEDOT:PSS/PVK/PC_{60}BM/LiF/Al	1.10	15.28	77.34	12.95[61]	Unencapsulated devices showed no change in performance for 20 days in an ambient air with 45% RH.

HDAPbI$_4$	1	2.44	FTO/c-TiO$_2$/PVK/Spiro/Ag	0.72	1.735	47.1	0.592[95]	Devices retained 57.3% after 96 h.
HDAMA$_4$Pb$_5$I$_{16}$	5	-	ITO/PEDOT:PSS/PVK/PC$_{60}$BM/LiF/Al	0.99	13.43	79	10.55[61]	Unencapsulated devices remained ~ 60% of their initial PCE for 20 days in an ambient air with 45% RH.
ODAPbI$_4$	1	2.55	FTO/c-TiO$_2$/PVK/Spiro/Ag	0.73	0.047	34	0.012[95]	N/A
PDMAPbI$_4$	1	2.42	FTO/c-TiO$_2$/mp-TiO$_2$/PVK/Spiro/Au	0.94	2.12	45	0.91[97]	N/A
PDMAFAPb$_2$I$_7$	2	-	FTO/c-TiO$_2$/mp-TiO$_2$/PVK/Spiro/Au	0.87	5.09	64.7	2.91[97]	N/A
PDMAFA$_2$Pb$_3$I$_{10}$	3	-	FTO/c-TiO$_2$/mp-TiO$_2$/PVK/Spiro/Au	0.84	10.83	71	6.46[97]	Unencapsulated devices maintained over 85% of the initial PCE after 60 days under dark ambient air (30-50% RH) and ambient temperature.
PDMAFA$_3$Pb$_4$I$_{13}$	4	1.51	FTO/c-TiO$_2$/mp-TiO$_2$/PVK/Spiro/Au	0.84	11.49	72.1	7.11[97]	N/A
PDMAA_9Pb$_{10}$(I$_{0.93}$Br$_{0.07}$)$_{31}$[b]	10	-	FTO/c-TiO$_2$/mp-TiO$_2$/PVK/Spiro/Au	1.02	21.5	71	15.6[63]	Unencapsulated devices only kept 20% of their initial efficiency after 84 h under ambient air (20%-50% RH).

[a] PVK represents perovskites; [b] average values; [c] Spiro: 2,2′,7,7′-Tetrakis[N,N-di(4-methoxyphenyl)amino]-9,9′-spirobifluorene; [d] *A* represents Cs$_{0.05}$MA$_{0.15}$FA$_{0.8}$; [e]Spacer cation is underlined in first row

Replacing the environmental unfriendly and toxic lead with other less-toxic or environmental benign metal is an effective approach to meet regulator's requirements for emerging applications. Among lead-free perovskites, Sn-based PSCs showed competitive opto-electrical properties, ideal optical bandgap around 1.33 eV and high charge carrier mobility.[98,99] However, the prompt Sn^{2+}/Sn^{4+} oxidation in 3-dimensional Sn-based perovskite limits their practical application.[100] Layered Sn-based DJ PSCs with improved stability was reported by Padture and co-workers.[94] The $4AMPFA_3Sn_4I_{13}$ ($n = 4$) perovskite possesses an extended absorption spectrum to 840 nm and long carrier lifetime (18.57 ns), which is significantly longer than those reported for Sn-based perovskite.[101] $4AMPFA_3Sn_4I_{13}$ was successfully integrated for solar cells fabrication with printable hole-transporting layer-free in a mesoscopic architecture and measured a promising PCE of 4.22% (Figure 6h & 6i). Significantly, the un-encapsulated PSCs with $4AMPFA_3Sn_4I_{13}$ can preserve 91% of initial efficiency after exposing to 1 sun illumination in an N_2 atmosphere at 45 °C for 100 h.

3.2 Alkyl-chain diamine

In typical layered 2D perovskite, the highly conductive inorganic slabs are separated by insulating large organic cation spacer leading to the quantum confinement effect and inhibits charge transport across the inorganic layers. The degree of quantum confinement as well as optical band gap can be determined by the number of the inorganic layer, *n* as well as the organic barrier length and cation charge. As the *n* value increases, the optical band gap decreases as a result of expansion of electronic band and thus the degree of quantum confinement decreases, which can approach to ABX_3 (3-dimensional) structure having infinite value of *n*. To select an appropriate length of spacer cation is one of the practical way to fine-tune the optoelectronic properties of DJ perovskite. By Increasing, the cation length can bring changes in electron and hole confinement potentials due to

structure distortion, which have a direct influence on the band gap of the perovskite and affects the charge transport efficiency.

In DJ perovskite, the organic cation and inorganic layer are bound together by electrostatic interactions between the ammonium end group at both end and the iodide anions. Long linear alkyl ammonium cations (7-9 carbon) tend to form staggered configuration with the long chain adopting the folded conformation (lower surface energy), and the inorganic layers are slight offset by half $[PbI_6]^{4-}$ octahedron tilted out of the plane due to strong hydrogen bonding; while the short alkyl chain(3-4carbon), tend to form eclipsed stacking arrangement. Further reducing interlayer distance (2 Å) by using a short dication such as propane-1,3-diammonium (PDA) may allow to reduce the quantum confinement as well, significantly enhancing interlayer charge transfer.

The DJ $PDAMA_3Pb_4I_{13}$-based PSCs in planar *p-i-n* structure yielded a PCE of 13.0%.[60] Additional moisture and thermal stability of layered PDA cation based PSCs are significantly improved as compared with BA cation based PSCs. PDA cation-based layered DJ PSC retained 90% of its original PCE, while BA cation-based layered RP PSCs decreases to 40% of its original value after 1000 h.

Recently, Li *et.al* systemically studied the stability of un-encapsulated devices and thin films based on $MAPbI_3$, RP $(PA)_2(MA)_3Pb_4I_{13}$ (PA: propylamine) and DJ $(PDA)(MA)_3Pb_4I_{13}$ perovskites under harsh environmental condition *i.e*. humidity, heat and light conditions (**Figure 7**).[64] DJ PSCs retained more than 95% initial efficiency aging for 4000 h at constant 40-70% RH, and constant 85 °C and 40-70% RH at the same time. Whereas the 3-dimensional and RP-based counterparts lost over 70% and 95% of their initial PCE, respectively. Further, these devices under constant 85/85 aging measurement (meaning 85 °C and 85% RH) showed similar behavior. The DJ $(PDA)(MA)_3Pb_4I_{13}$ tolerated more than 95% PCE after continuous light soaking for 3,000

h while $MAPbI_3$, RP $(PA)_2(MA)_3Pb_4I_{13}$ PSCs were able to kept 20% and 60% of their original efficiencies only. However, the exposure time of the 85/85 aging measurement was not sufficient to meet the strict requirements for PV stability by the International Electrotechnical Commission IEC61215:2016 standard (1,000 h at 85/85 aging condition). The use of spacer cations having the hydrophobic and insulating natures can increase tolerant to humidity on the devices, which will allow achieving higher stability than 3D. By eliminating van der Waals gap and replacing it with hydrogen bonds between the spacer cations and perovskite slabs, DJ perovskite are able to form stable crystal structure and improved performance than of RP perovskites.[102]

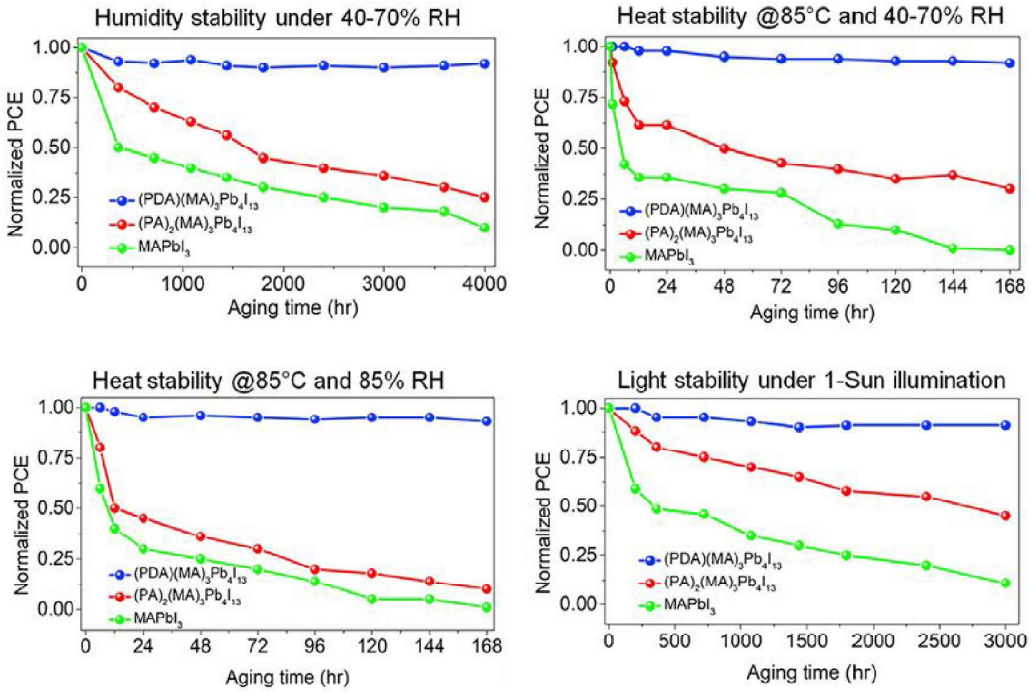

Figure 7. Stability testing of 3D $MAPbI_3$, RP $(PA)_2(MA)_3Pb_4I_{13}$ and DJ $(PDA)(MA)_3Pb_4I_{13}$-based perovskite solar cells under harsh humidity, heat and light conditions. Reprinted with permission from reference 64. Copyright 2019 Elsevier.

Recently, Huang and co-workers systematically investigated a series of DJ perovskite ($n = 5$) by comparing large numbers of chain lengths of spacer cations (e.g., PDA, BDA, PeDA, and HDA).[61] As shown in optical absorption spectra (**Figure 8a)**, additional peaks

at 610 and 640 nm in PeDA-based perovskites and 590 nm in HDA was observed, the excitonic peak in PDA- and BDA-based DJ- perovskites were not prominent, as the alkyl chain spacers reduces the distortion of crystal structure, thereby exhibiting a relatively uniform QW distribution (Figure 8b).[103,104] The PDA- and BDA- based DJ perovskites showed stronger and sharper discrete Bragg spots than of PeDA- and HDA-based films (Figure 8c), indicating that the highly oriented crystal growth could be controlled by spacer cations with short-chain lengths.[105,106] DJ perovskites based on PDA and BDA cation have uniform QW distribution and vertically aligned crystal orientation, which can decrease defect densities, charge mobilities and thus final performance of devices. Finally, the planar *p-i-n* devices were fabricated based on PDA and BDA cation, which gave an improve performance of 14.8% and 16.4%, respectively, as compared with 12.95% and 10.55% of PCEs obtained from analogous devices using PeDA and HDA, respectively (Figure 8d & 8e). A high PCE of 17.91% was achieved with the optimized device based on BDA as a spacer cation, which is the highest value for DJ PSCs reported so far. (Figure 8f).[62] The long-term stability of BDA-, BA- based layered and 3D PSCs without any encapsulation under ambient conditions with a relative humidity of ~60% were tested (Figure 8f). The BDA based devices showed the best stability and preserved 84% of its original PCE after1182 h, while the device with BA cation and 3D perovskites showed 73% and 39% of their initial PCE after 1176 h and 1008 h respectively. [62] Though the DJ phase having alkyl-chain diamine based PSCs achieved higher efficiency, report on crystal structure and alignment of spacer cations in the structure is unavailable, this demands investigation of crystal structure of DJ perovskite having alkyl-chain diamine.

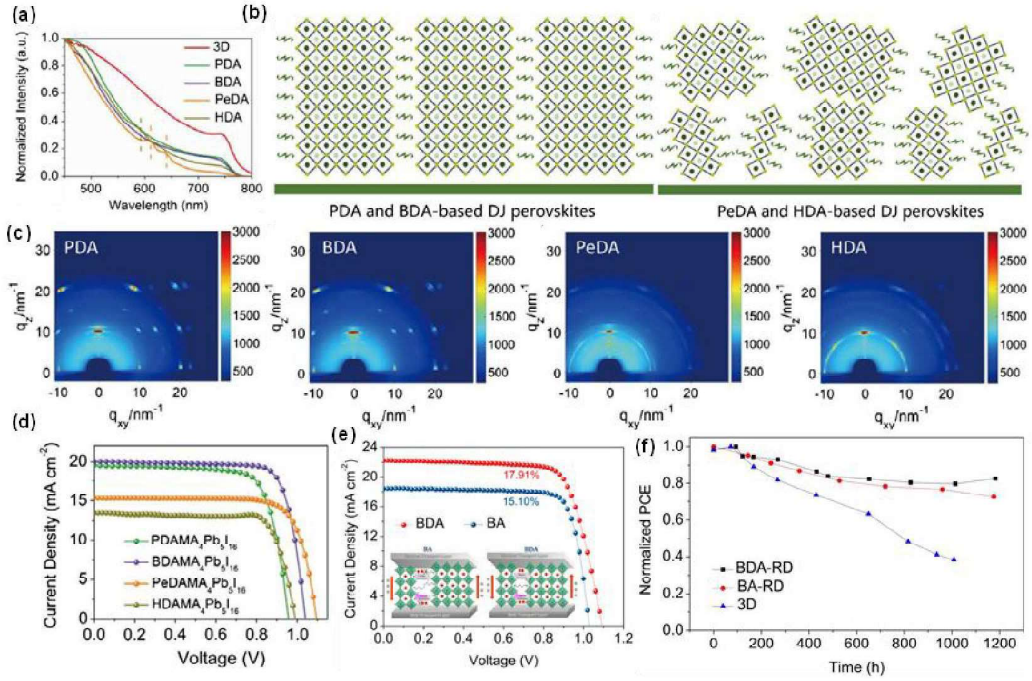

Figure 8. (a) Absorption of DJ perovskite with different spacer cations, (b) Schematic diagram of the homogeneous and multiphase DJ perovskites, (c) GIWAXS maps for DJ perovskites with different spacer cations, (d) *J*–*V* curves of devices with different DJ perovskites, (e) *J*–*V* curves of the champion DJ PSC with BDA as a spacer cation. Reprinted with permission from reference 61. Copyright 2019 Wiley-VCH. (f) Device stability of PCE in ambient air without any encapsulation of BDA-RD, BA-RD, and 3D PSCs. *J*–*V* curve of champion PSC device with BDA and BA as spacer cations. Reproduced from reference 62. Copyright 2019 American Chemical Society.

3.3 Benzene Dimethanammonium

Grätzel and co-workers were the first to employ PDMA as a spacer cation in DJ based perovskites using formamidinium (FA) as A-site organic cation and reported PCE of >7% for PDMA $FA_2Pb_3I_{10}$-based PSCs in a mesoporous device structure.[97] It is worth mentioning that the preparation of DJ films at room temperature in the absence of additives and antisolvents varied from previous reports of using hot-casting or anti-solvent methods for thin-film fabrication.[61,62,64] Importantly, the electron mobility was

comparable to those reported for the hot-casting deposition method. In addition, the device showed higher stability under humidity and light illumination conditions. Recently, Etgar *et.al* were able to push the performance of DJ PSCs with PDMA as a spacer cation to 15.6% via tailoring *n* values to 10 and mixed A-site cations and X site ions.[63] The favorable band alignment of DJ perovskite to the charge selective contacts allow improved charge extraction and increases the inner potentials, which can enhance the overall voltage of devices and support the long separation of charge carrier in the active layer.[107] However in case of DJ perovskite with $n = 10$, the stability merits of layered perovskite based devices is sacrificed, and it is worthy to balance this tradeoff of stability and performance through systematic studies.

4. Outlook and Future Perspectives

Here, we summarized the breakthroughs made in recent years in the field of Dion-Jacobson layered PSCs, the fabricated solar cells employing Dion-Jacobson perovskites yielded the highest efficiency of 17.9%, along with improved long-term stability under ambient conditions without encapsulation (the Dion-Jacobson layered PSCs retained 84% % of initial PCE under 60% RH after 1182 h, while 3D PSCs retained their initial PCE of 39% after 1008 h). These preliminary results suggests that Dion-Jacobson layered perovskite has a competitive edge for commercial endeavor of perovskite. However, the efficiency of Dion-Jacobson layered PSCs lag behind the 3D counterparts (25.2%). By adopting the following measures, it allows fine-tuning the investigation and exploiting such materials for efficient solar cells fabrication.

Benign and facile process to fabricate high-quality Dion-Jacobson layered perovskite films with preferred crystal orientation is of paramount importance. In this direction, the hot-casting process can allow inducing high crystal orientation in Dion-Jacobson layered films, but the high-temperature annealing post-spin-coating process (>

100 ℃) may restrict the fundamental research and application for large-area or flexible solar cells fabrication. Using anti-solvents, such as chlorobenzene, can be a simple mean to induce high orientation in perovskite films, however, the usage of toxic solvents and process drawbacks will hinder the application of Dion-Jacobson layered PSCs. If we take into account that the properties of the bottom transport layer affects the crystallization process of perovskites, the employment of rational charge selective layers/interface modification for optimizing contact angle or surface energy will be an effective way to fabricate Dion-Jacobson perovskite with the preferred crystal orientation. Besides this, adjusting the intermediate phase of perovskite precursors via introducing new solvents, tuning the ratio and doping other materials will realize high-quality Dion-Jacobson layered perovskite.

The layered/low dimensional perovskite is vastly tolerant to spacer cations giving a choice of a wide variety of sizes and functional groups, this potentially paves the way to virtually infinite chemistry. However, the possibility in case of integrated diamine spacer cations of Dion-Jacobson perovskite for solar cells is limited, and only three types of spacer cations (piperidinium derivatives, alkyl-chain diamine, and benzene dimethanammonium) used in the Dion-Jacobson PSCs. Introducing unique diamine spacer cations with π-conjugated functional unit will be a possible strategy to prepare Dion-Jacobson layered perovskite with excellent electro-optical properties. Ideally to be used as successful spacer cation for Dion-Jacobson layered in solar cells should follow the following selection criteria, (i) the hydrogen bonding between spacer cations and perovskite slabs have an impact on in-plane *B-X-B*, such as *Pb-I-Pb* angles, which are directly correlated to the electro-optical properties of Dion-Jacobson perovskites. The new spacer cation forming hydrogen bonding with perovskite slabs, should not contribute to the in-plane *B-X-B* distortion and ensure the more linear *B-X-B* angles (closer to 180°).

The *B-X-B* angle needs to control the components of perovskite slabs. When introducing new spacer cations, it is essential to tune the components of perovskite slabs to optimize the opto-electrical properties of Dion-Jacobson layered perovskite. (ii) appropriate quantum well barrier thickness plays a vital role in the charge carrier transport in Dion-Jacobson layer, this in turn, allows to achieve excellent orientation and uniform quantum well distribution and permit a smooth bandgap transition. Such characteristics will favor longer carrier diffusion length, higher charge mobility, and low defect density. The introduction of new short length spacer cations having aromatic ring for Dion-Jacobson layered PSCs, can provide more rigidity to the cation, more delocalization of π-electrons, and high dielectric constant of the aromatic cation as compared to their aliphatic analogues. This will allow to have smaller dielectric confinement effect with small exciton binding energy to induce a better charge separation and transportation in PSCs. Inspired by the functional spacer cations of Ruddlesden−Popper perovskites, such as 2,2,2-trifluoroethylamine, 2-(4-fluorophenyl)ethyl ammonium, and 2-thiophenemethylammonium (ThMA) cations, introducing diamine spacer cations having functional unit such as π-conjugated oligothiophene, terthiophene, *etc*. is a possible strategy to prepare Dion-Jacobson layered perovskite with excellent PV and light emission properties. Phase-pure Dion-Jacobson perovskite with $n > 2$ is still challenging because the thermodynamic instability of the 2-dimensional phases was found to decrease with increasing *n* values,[68] also, the charge carrier transportation will be limited between the spacer cation layers or by the charge trapping at the low-n components. Investigation of crystal and growth mechanism of phase-pure perovskite with high n values understanding is vital to obtain Dion-Jacobson layered perovskite with controlled composition/structures and enhanced crystalline phase purity.

The Dion-Jacobson layered PSCs represented enhanced stability under harsh environmental condition *i.e.* humidity, heat and light conditions for aliphatic diammonium cation(n = 4), however, for aromatic diammonium cation (n = 4), the stability report is lacking. The solar cells with competitive stability under different stress conditions such as moisture, heat and light illumination instead of only practical conditions are prerequisites, and it is worth to assess the stability performance under different conditions. A probable solution to improve the long-term, operational stability of Dion-Jacobson layered PSCs under complicated conditions can be the replacement of the A-site organic cation (MA^+, FA^+) with inorganic cation such as Cs^+, Rb^+ or their mixed alloy. The potential perovskite should combine the advantages of moisture stability of Dion-Jacobson layered perovskite and heat resistivity of all-inorganic perovskite. More importantly, intrinsic stability such as thermodynamic and mechanical stability ensure the device can tolerate external environment is urgently required. Perovskite slabs (n above a critical value) in layered perovskites trigger the relaxation of the interface strain. This leads to the release of the mechanical energy arising from the lattice mismatch, which might potentially induce the formation of lower energy states, playing a crucial role in the design of novel layered perovskite with unique intrinsic stability.[108] More importantly, PSCs can be fabricated employing non-toxic Sn- or having similar physio-chemical properties-based perovskite for replacement of lead-based PSCs. There exists a trade-off, as the 3-dimensional Sn-based PSCs exhibits poor atmospheric stability in high humid condition, however, due to spacer cations of Dion-Jacobson perovskite, Sn-based Dion-Jacobson PSCs can be an important contender for future PV applications.

Author Information

ORCID Peng Huang: 0000-0002-5150-8213

Samrana Kazim: 0000-0003-2684-2209

Mingkui Wang: 0000-0002-4516-2500

Shahzada Ahmad: 0000-0002-1218-2556

Notes

The authors declare no conflict of interest.

Biographies

Peng Huang is a postdoctoral researcher in Prof. Shahzada Ahmad´s group at BCMaterials in Spain. He received his Ph.D. from Soochow University, China (2018). His research focuses on the interface engineering for perovskite solar cells and low-dimensional/layered perovskites.

Samrana Kazim is Ikerbasque fellow and group leader at BCMaterials focusing on developing novel nanostructured materials and hybrid inorganic-organic solar cells. She completed her Ph.D. in 2008 and worked at Institute of Macromolecular Chemistry and as a tenured senior scientist (2013-2017) at a corporate research center of Abengoa.

Mingkui Wang is a professor at Huazhong University of Science and Technology. He received his Ph.D. from CCIAC, China and worked as Humboldt fellow at TUM, Germany and post-doctoral researcher at EPFL. His research interests are developing next-generation solar cells and applying electrochemistry to elucidation of fundamental phenomena in photonics.

Shahzada Ahmad is Ikerbasque professor at BCMaterials working on innovative materials for energy application. He was Humboldt fellow at Max Planck institute and studied interfaces by scanning probe microscopy, at EPFL he developed nanoporous

electrode for metal free electro-catalysis, and as a program director of photovoltaics at Abengoa research.

Acknowledgements

This work has received funding from the European Union H2020 Programme under European Research council Consolidator grant [MOLEMAT, 726360] and Spanish ministry of Science and Technology. Financial support from the National Natural Science Foundation of China Major International (Regional) Joint Research Project (NO. 51661135023, 51961165106), National Natural Science Foundation of China (No. 21673091, 21975088) are acknowledged.

Reference

(1) Kojima, A.; Teshima, K.; Shirai, Y.; Miyasaka, T. Organometal Halide Perovskites as Visible-Light Sensitizers for Photovoltaic Cells. *J. Am. Chem. Soc.* **2009**, *131* (17), 6050–6051.

(2) Zhou, H.; Chen, Q.; Li, G.; Luo, S.; Song, T. B.; Duan, H. S.; Hong, Z.; You, J.; Liu, Y.; Yang, Y. Interface Engineering of Highly Efficient Perovskite Solar Cells. *Science.* **2014**, *345* (6196), 542–546.

(3) Grätzel, M. The Rise of Highly Efficient and Stable Perovskite Solar Cells. *Acc. Chem. Res.* **2017**, *50* (3), 487–491.

(4) Burschka, J.; Pellet, N.; Moon, S.-J. J.; Humphry-Baker, R.; Gao, P.; Nazeeruddin, M. K.; Grätzel, M. Sequential Deposition as a Route to High-Performance Perovskite-Sensitized Solar Cells. *Nature* **2013**, *499* (7458), 316–319.

(5) Jiang, Q.; Zhao, Y.; Zhang, X.; Yang, X.; Chen, Y.; Chu, Z.; Ye, Q.; Li, X.; Yin, Z.; You, J. Surface Passivation of Perovskite Film for Efficient Solar Cells. *Nat. Photonics* **2019**, *13* (7), 460–466.

(6) Liu, M.; Johnston, M. B.; Snaith, H. J. Efficient Planar Heterojunction Perovskite Solar Cells by Vapour Deposition. *Nature* **2013**, *501* (7467), 395–398.

(7) Bai, S.; Da, P.; Li, C.; Wang, Z.; Yuan, Z.; Fu, F.; Kawecki, M.; Liu, X.; Sakai, N.; Wang, J. T.-W. W.; Huettner, S.; Buecheler, S.; Fahlman, M.; Gao, F.; Snaith, H. J. Planar Perovskite Solar Cells with Long-Term Stability Using Ionic Liquid Additives. *Nature* **2019**, *571* (7764), 245–250.

(8) Kim, H.-S.; Lee, C.-R.; Im, J.-H.; Lee, K.-B.; Moehl, T.; Marchioro, A.; Moon, S.-J.; Humphry-Baker, R.; Yum, J.-H.; Moser, J. E.; Grätzel, M.; Park, N.-G. Lead Iodide Perovskite Sensitized All-Solid-State Submicron Thin Film Mesoscopic Solar Cell with Efficiency Exceeding 9%. *Sci. Rep.* **2012**, *2* (1), 591.

(9) Hu, M.; Bi, C.; Yuan, Y.; Xiao, Z.; Dong, Q.; Shao, Y.; Huang, J. Distinct Exciton Dissociation Behavior of Organolead Trihalide Perovskite and Excitonic Semiconductors Studied in the Same System. *Small* **2015**, *11* (18), 2164–2169.

(10) Zheng, L.; Ma, Y.; Chu, S.; Wang, S.; Qu, B.; Xiao, L.; Chen, Z.; Gong, Q.; Wu, Z.; Hou, X. Improved Light Absorption and Charge Transport for Perovskite Solar Cells with Rough Interfaces by Sequential Deposition. *Nanoscale* **2014**, *6* (14), 8171–8176.

(11) Xie, F.; Chen, C. C.; Wu, Y.; Li, X.; Cai, M.; Liu, X.; Yang, X.; Han, L. Vertical Recrystallization for Highly Efficient and Stable Formamidinium-Based Inverted-Structure Perovskite Solar Cells. *Energy Environ. Sci.* **2017**, *10* (9), 1942–1949.

(12) Xing, G.; Mathews, N.; Sun, S.; Lim, S. S.; Lam, Y. M.; Graẗzel, M.; Mhaisalkar, S.; Sum, T. C. Long-Range Balanced Electron-and Hole-Transport Lengths in Organic-Inorganic CH3NH3PbI3. *Science.* **2013**, *342* (6156), 344–347.

(13) Shi, D.; Adinolfi, V.; Comin, R.; Yuan, M.; Alarousu, E.; Buin, A.; Chen, Y.; Hoogland, S.; Rothenberger, A.; Katsiev, K.; Losovyj, Y.; Zhang, X.; Dowben, P. A.; Mohammed, O. F.; Sargent, E. H.; Bakr, O. M. Low Trap-State Density and Long Carrier Diffusion in Organolead Trihalide Perovskite Single Crystals. *Science.* **2015**, *347* (6221), 519–522.

(14) Dong, Q.; Fang, Y.; Shao, Y.; Mulligan, P.; Qiu, J.; Cao, L.; Huang, J. Electron-Hole Diffusion Lengths > 175 Mm in Solution-Grown CH3NH3PbI3 Single Crystals. *Science.* **2015**, *347* (6225), 967–970.

(15) Stranks, S. D.; Eperon, G. E.; Grancini, G.; Menelaou, C.; Alcocer, M. J. P.; Leijtens, T.; Herz, L. M.; Petrozza, A.; Snaith, H. J.; Stranks, S. D.; Eperon, G. E.; Grancini, G.; Menelaou, C.; Alcocer, M. J. P.; Leijtens, T.; Herz, L. M.; Petrozza, A.; Snaith, H. J.; Stranks, S. D.; et al. Electron-Hole Diffusion Lengths Exceeding 1 Micrometer in an Organometal Trihalide Perovskite Absorber. *Science.* **2013**, *342* (6156), 341–344.

(16) Oga, H.; Saeki, A.; Ogomi, Y.; Hayase, S.; Seki, S. Improved Understanding of the Electronic and Energetic Landscapes of Perovskite Solar Cells: High Local Charge Carrier Mobility, Reduced Recombination, and Extremely Shallow Traps.

J. Am. Chem. Soc. **2014**, *136* (39), 13818–13825.

(17) Cao, T.; Huang, P.; Zhang, K.; Sun, Z.; Zhu, K.; Yuan, L.; Chen, K.; Chen, N.; Li, Y. Interfacial Engineering via Inserting Functionalized Water-Soluble Fullerene Derivative Interlayers for Enhancing the Performance of Perovskite Solar Cells. *J. Mater. Chem. A* **2018**, *6* (8), 3435–3443.

(18) Salado, M.; Jodlowski, A. D.; Roldan-Carmona, C.; de Miguel, G.; Kazim, S.; Nazeeruddin, M. K.; Ahmad, S. Surface Passivation of Perovskite Layers Using Heterocyclic Halides: Improved Photovoltaic Properties and Intrinsic Stability. *Nano Energy* **2018**, *50*, 220–228.

(19) Kazim, S.; Nazeeruddin, M. K.; Grätzel, M.; Ahmad, S. Perovskite as Light Harvester: A Game Changer in Photovoltaics. *Angew. Chemie - Int. Ed.* **2014**, *53* (11), 2812–2824.

(20) Nie, W.; Tsai, H.; Asadpour, R.; Blancon, J.-C.; Neukirch, A. J.; Gupta, G.; Crochet, J. J.; Chhowalla, M.; Tretiak, S.; Alam, M. A.; Wang, H.-L.; Mohite, A. D. High-Efficiency Solution-Processed Perovskite Solar Cells with Millimeter-Scale Grains. *Science.* **2015**, *347* (6221), 522–525.

(21) You, J.; Hong, Z.; Yang, Y. (Michael); Chen, Q.; Cai, M.; Song, T.; Chen, C.; Lu, S.; Liu, Y.; Zhou, H.; Yang, Y. Low-Temperature Solution-Processed Perovskite Solar Cells with High Efficiency and Flexibility. *ACS Nano* **2014**, *8* (2), 1674–1680.

(22) Liu, X.; Huang, P.; Dong, Q.; Wang, Z.; Zhang, K.; Yu, H.; Lei, M.; Zhou, Y.; Song, B.; Li, Y. Enhancement of the Efficiency and Stability of Planar P-i-n Perovskite Solar Cells via Incorporation of an Amine-Modified Fullerene Derivative as a Cathode Buffer Layer. *Sci. China Chem.* **2017**, *60* (1), 136–143.

(23) NREL, Best Research-Cell Efficiencies. *https://www.nrel.gov/pv/cell-efficiency.html* (accessed: July 2019).

(24) Ke, W.; Kanatzidis, M. G. Prospects for Low-Toxicity Lead-Free Perovskite Solar Cells. *Nat. Commun.* **2019**, *10* (1), 965.

(25) Lyu, M.; Yun, J.-H. H.; Chen, P.; Hao, M.; Wang, L. Addressing Toxicity of Lead: Progress and Applications of Low-Toxic Metal Halide Perovskites and Their Derivatives. *Adv. Energy Mater.* **2017**, *7* (15), 1602512.

(26) Leijtens, T.; Eperon, G. E.; Noel, N. K.; Habisreutinger, S. N.; Petrozza, A.; Snaith, H. J. Stability of Metal Halide Perovskite Solar Cells. *Adv. Energy Mater.* **2015**, *5* (20), 1500963.

(27) Arabpour Roghabadi, F.; Alidaei, M.; Mousavi, S. M.; Ashjari, T.; Tehrani, A. S.; Ahmadi, V.; Sadrameli, S. M. Stability Progress of Perovskite Solar Cells Dependent on the Crystalline Structure: From 3D ABX_3 to 2D Ruddlesden-Popper Perovskite Absorbers. *J. Mater. Chem. A* **2019**, *7* (11), 5898–5933.

(28) Zhou, Y.; Zhao, Y. Chemical Stability and Instability of Inorganic Halide Perovskites. *Energy Environ. Sci.* **2019**, *12* (5), 1495–1511.

(29) Shalan, A. E.; Kazim, S.; Ahmad, S. Lead-Free Perovskites: Metals Substitution towards Environmentally Benign Solar Cell Fabrication. *ChemSusChem* **2019**, *12* (18), 4116–4139.

(30) Wang, K.; Jin, Z.; Liang, L.; Bian, H.; Wang, H.; Feng, J.; Wang, Q.; Liu, S. (Frank). Chlorine Doping for Black γ-$CsPbI_3$ Solar Cells with Stabilized Efficiency beyond 16%. *Nano Energy* **2019**, *58*, 175–182.

(31) Wang, L.; Zhou, H.; Hu, J.; Huang, B.; Sun, M.; Dong, B.; Zheng, G.; Huang, Y.; Chen, Y.; Li, L.; Xu, Z.; Li, N.; Liu, Z.; Chen, Q.; Sun, L.-D.; Yan, C.-H. A Eu^{3+}-Eu^{2+} Ion Redox Shuttle Imparts Operational Durability to Pb-I Perovskite Solar Cells. *Science.* **2019**, *363* (6424), 265–270.

(32) Xiang, W.; Wang, Z.; Kubicki, D. J.; Tress, W.; Luo, J.; Prochowicz, D.; Akin, S.; Emsley, L.; Zhou, J.; Dietler, G.; Grätzel, M.; Hagfeldt, A. Europium-Doped $CsPbI_2Br$ for Stable and Highly Efficient Inorganic Perovskite Solar Cells. *Joule* **2019**, *3* (1), 205–214.

(33) Duan, J.; Zhao, Y.; Yang, X.; Wang, Y.; He, B.; Tang, Q. Lanthanide Ions Doped CsPbBr 3 Halides for HTM-Free 10.14%-Efficiency Inorganic Perovskite Solar Cell with an Ultrahigh Open-Circuit Voltage of 1.594 V. *Adv. Energy Mater.* **2018**, *8* (31), 1802346.

(34) Yan, W.; Rao, H.; Wei, C.; Liu, Z.; Bian, Z.; Xin, H.; Huang, W. Highly Efficient and Stable Inverted Planar Solar Cells from $(FAI)_x(MABr)_{1-x}PbI_2$ perovskites. *Nano Energy* **2017**, *35*, 62–70.

(35) Salado, M.; Shirzadi, E.; Kazim, S.; Fei, Z.; Nazeeruddin, M. K.; Dyson, P. J.; Ahmad, S. Oxazolium Iodide Modified Perovskites for Solar Cell Fabrication. *ChemPluschem* **2018**, *83* (4), 279–284.

(36) Jodlowski, A. D.; Roldán-Carmona, C.; Grancini, G.; Salado, M.; Ralaiarisoa, M.; Ahmad, S.; Koch, N.; Camacho, L.; De Miguel, G.; Nazeeruddin, M. K. Large Guanidinium Cation Mixed with Methylammonium in Lead Iodide Perovskites for 19% Efficient Solar Cells. *Nat. Energy* **2017**, *2* (12), 972–979.

(37) Jeon, N. J.; Noh, J. H.; Yang, W. S.; Kim, Y. C.; Ryu, S.; Seo, J.; Seok, S. Il. Compositional Engineering of Perovskite Materials for High-Performance Solar Cells. *Nature* **2015**, *517* (7535), 476–480.

(38) Grancini, G.; Roldán-Carmona, C.; Zimmermann, I.; Mosconi, E.; Lee, X.; Martineau, D.; Narbey, S.; Oswald, F.; De Angelis, F.; Graetzel, M.; Nazeeruddin, M. K. One-Year Stable Perovskite Solar Cells by 2D/3D Interface Engineering. *Nat. Commun.* **2017**, *8* (14), 15684.

(39) Huang, P.; Chen, Q.; Zhang, K.; Yuan, L.; Zhou, Y.; Song, B.; Li, Y. 21.7% Efficiency Achieved in Planar N–i–p Perovskite Solar Cells via Interface Engineering with Water-Soluble 2D TiS_2. *J. Mater. Chem. A* **2019**, *7* (11), 6213–6219.

(40) Agresti, A.; Pescetelli, S.; Palma, A. L.; Del Rio Castillo, A. E.; Konios, D.; Kakavelakis, G.; Razza, S.; Cinà, L.; Kymakis, E.; Bonaccorso, F.; Di Carlo, A. Graphene Interface Engineering for Perovskite Solar Modules: 12.6% Power Conversion Efficiency over 50 cm^2 Active Area. *ACS Energy Lett.* **2017**, *2* (1), 279–287.

(41) Chen, W.; Xu, L.; Feng, X.; Jie, J.; He, Z. Metal Acetylacetonate Series in Interface Engineering for Full Low-Temperature-Processed, High-Performance, and Stable Planar Perovskite Solar Cells with Conversion Efficiency over 16% on 1 cm^2 Scale. *Adv. Mater.* **2017**, *29* (16), 1603923.

(42) Huang, P.; Wang, Z.; Liu, Y.; Zhang, K.; Yuan, L.; Zhou, Y.; Song, B.; Li, Y. Water-Soluble 2D Transition Metal Dichalcogenides as the Hole-Transport Layer for Highly Efficient and Stable p-i-n Perovskite Solar Cells. *ACS Appl. Mater. Interfaces* **2017**, *9* (30), 25323–25331.

(43) Huang, P.; Yuan, L.; Zhang, K.; Chen, Q.; Zhou, Y.; Song, B.; Li, Y. Room-Temperature and Aqueous Solution-Processed Two-Dimensional TiS2 as an Electron Transport Layer for Highly Efficient and Stable Planar N–i–p Perovskite Solar Cells. *ACS Appl. Mater. Interfaces* **2018**, *10* (17), 14796–14802.

(44) Zhang, J.; Xu, L. J.; Huang, P.; Zhou, Y.; Zhu, Y. Y.; Yuan, N. Y.; Ding, J. N.; Zhang, Z. G.; Li, Y. F. A Simple and Dopant-Free Hole-Transporting Material Based on (2-Ethylhexyl)-9 H -Carbazole for Efficient Planar Perovskite Solar Cells. *J. Mater. Chem. C* **2017**, *5* (48), 12752–12757.

(45) Caliò, L.; Follana-Berná, J.; Kazim, S.; Madsen, M.; Rubahn, H.-G.; Sastre-Santos, Á.; Ahmad, S. Cu(II) and Zn(II) Based Phthalocyanines as Hole Selective Layers

for Perovskite Solar Cells. *Sustain. Energy Fuels* **2017**, *1* (10), 2071–2077.

(46) Daskeviciene, M.; Paek, S.; Wang, Z.; Malinauskas, T.; Jokubauskaite, G.; Rakstys, K.; Cho, K. T.; Magomedov, A.; Jankauskas, V.; Ahmad, S.; Snaith, H. J.; Getautis, V.; Nazeeruddin, M. K. Carbazole-Based Enamine: Low-Cost and Efficient Hole Transporting Material for Perovskite Solar Cells. *Nano Energy* **2017**, *32*, 551–557.

(47) Caliò, L.; Salado, M.; Kazim, S.; Ahmad, S. A Generic Route of Hydrophobic Doping in Hole Transporting Material to Increase Longevity of Perovskite Solar Cells. *Joule* **2018**, *2* (9), 1800–1815.

(48) Idígoras, J.; Aparicio, F. J.; Contreras-Bernal, L.; Ramos-Terrón, S.; Alcaire, M.; Sánchez-Valencia, J. R.; Borras, A.; Barranco, Á.; Anta, J. A. Enhancing Moisture and Water Resistance in Perovskite Solar Cells by Encapsulation with Ultrathin Plasma Polymers. *ACS Appl. Mater. Interfaces* **2018**, *10* (14), 11587–11594.

(49) Wong-Stringer, M.; Game, O. S.; Smith, J. A.; Routledge, T. J.; Alqurashy, B. A.; Freestone, B. G.; Parnell, A. J.; Vaenas, N.; Kumar, V.; Alawad, M. O. A. A.; Iraqi, A.; Rodenburg, C.; Lidzey, D. G. High-Performance Multilayer Encapsulation for Perovskite Photovoltaics. *Adv. Energy Mater.* **2018**, *8* (24), 1801234.

(50) Bi, E.; Chen, H.; Xie, F.; Wu, Y.; Chen, W.; Su, Y.; Islam, A.; Grätzel, M.; Yang, X.; Han, L. Diffusion Engineering of Ions and Charge Carriers for Stable Efficient Perovskite Solar Cells. *Nat. Commun.* **2017**, *8* (1), 15330.

(51) Tsai, H.; Nie, W.; Blancon, J. C.; Stoumpos, C. C.; Asadpour, R.; Harutyunyan, B.; Neukirch, A. J.; Verduzco, R.; Crochet, J. J.; Tretiak, S.; Pedesseau, L.; Even, J.; Alam, M. A.; Gupta, G.; Lou, J.; Ajayan, P. M.; Bedzyk, M. J.; Kanatzidis, M. G.; Mohite, A. D. High-Efficiency Two-Dimensional Ruddlesden-Popper Perovskite Solar Cells. *Nature* **2016**, *536* (7616), 312–317.

(52) Grancini, G.; Nazeeruddin, M. K. Dimensional Tailoring of Hybrid Perovskites for Photovoltaics. *Nat. Rev. Mater.* **2019**, *4* (1), 4–22.

(53) Mao, L.; Ke, W.; Pedesseau, L.; Wu, Y.; Katan, C.; Even, J.; Wasielewski, M. R.; Stoumpos, C. C.; Kanatzidis, M. G. Hybrid Dion-Jacobson 2D Lead Iodide Perovskites. *J. Am. Chem. Soc.* **2018**, *140* (10), 3775–3783.

(54) Stoumpos, C. C.; Soe, C. M. M.; Tsai, H.; Nie, W.; Blancon, J.-C.; Cao, D. H.; Liu, F.; Traoré, B.; Katan, C.; Even, J.; Mohite, A. D.; Kanatzidis, M. G. High Members of the 2D Ruddlesden-Popper Halide Perovskites: Synthesis, Optical Properties, and Solar Cells of $(CH_3(CH_2)_3NH_3)_2(CH_3NH_3)_4Pb_5I_{16}$. *Chem* **2017**, *2* (3), 427–440.

(55) Smith, I. C.; Hoke, E. T.; Solis-Ibarra, D.; McGehee, M. D.; Karunadasa, H. I. A Layered Hybrid Perovskite Solar-Cell Absorber with Enhanced Moisture Stability. *Angew. Chemie - Int. Ed.* **2014**, *53* (42), 11232–11235.

(56) Yang, R.; Li, R.; Cao, Y.; Wei, Y.; Miao, Y.; Tan, W. L.; Jiao, X.; Chen, H.; Zhang, L.; Chen, Q.; Zhang, H.; Zou, W.; Wang, Y.; Yang, M.; Yi, C.; Wang, N.; Gao, F.; McNeill, C. R.; Qin, T.; et al. Oriented Quasi-2D Perovskites for High Performance Optoelectronic Devices. *Adv. Mater.* **2018**, *30* (51), 1804771.

(57) Li, H.; Wang, X.; Zhang, T.; Gong, X.; Sun, Q.; Pan, H.; Shen, Y.; Ahmad, S.; Wang, M. Layered Ruddlesden–Popper Efficient Perovskite Solar Cells with Controlled Quantum and Dielectric Confinement Introduced via Doping. *Adv. Funct. Mater.* **2019**, *29* (30), 1903293.

(58) Quan, L. N.; Yuan, M.; Comin, R.; Voznyy, O.; Beauregard, E. M.; Hoogland, S.; Buin, A.; Kirmani, A. R.; Zhao, K.; Amassian, A.; Kim, D. H.; Sargent, E. H. Ligand-Stabilized Reduced-Dimensionality Perovskites. *J. Am. Chem. Soc.* **2016**, *138* (8), 2649–2655.

(59) Zhang, X.; Ren, X.; Liu, B.; Munir, R.; Zhu, X.; Yang, D.; Li, J.; Liu, Y.; Smilgies, D.-M.; Li, R.; Yang, Z.; Niu, T.; Wang, X.; Amassian, A.; Zhao, K.; Liu, S. F. Stable High Efficiency Two-Dimensional Perovskite Solar Cells via Cesium Doping. *Energy Environ. Sci.* **2017**, *10* (10), 2095–2102.

(60) Ma, C.; Shen, D.; Ng, T.-W.; Lo, M.-F.; Lee, C.-S. 2D Perovskites with Short Interlayer Distance for High-Performance Solar Cell Application. *Adv. Mater.* **2018**, *30* (22), 1800710.

(61) Zheng, Y.; Niu, T.; Qiu, J.; Chao, L.; Li, B.; Yang, Y.; Li, Q.; Lin, C.; Gao, X.; Zhang, C.; Xia, Y.; Chen, Y.; Huang, W. Oriented and Uniform Distribution of Dion–Jacobson Phase Perovskites Controlled by Quantum Well Barrier Thickness. *Sol. RRL* **2019**, 1900090.

(62) Niu, T.; Ren, H.; Wu, B.; Xia, Y.; Xie, X.; Yang, Y.; Gao, X.; Chen, Y.; Huang, W. Reduced-Dimensional Perovskite Enabled by Organic Diamine for Efficient Photovoltaics. *J. Phys. Chem. Lett.* **2019**, *10* (10), 2349–2356.

(63) Cohen, B.-E.; Li, Y.; Meng, Q.; Etgar, L. Dion–Jacobson Two-Dimensional Perovskite Solar Cells Based on Benzene Dimethanammonium Cation. *Nano Lett.* **2019**, *19* (4), 2588–2597.

(64) Ahmad, S.; Fu, P.; Yu, S.; Yang, Q.; Liu, X.; Wang, X.; Wang, X.; Guo, X.; Li, C. Dion-Jacobson Phase 2D Layered Perovskites for Solar Cells with Ultrahigh

Stability. *Joule* **2019**, *3* (3), 794–806.

(65) Saparov, B.; Mitzi, D. B. Organic-Inorganic Perovskites: Structural Versatility for Functional Materials Design. *Chem. Rev.* **2016**, *116* (7), 4558–4596.

(66) Li, X.; Ke, W.; Traoré, B.; Guo, P.; Hadar, I.; Kepenekian, M.; Even, J.; Katan, C.; Stoumpos, C. C.; Schaller, R. D.; Kanatzidis, M. G. Two-Dimensional Dion–Jacobson Hybrid Lead Iodide Perovskites with Aromatic Diammonium Cations. *J. Am. Chem. Soc.* **2019**, *141* (32), 12880–12890.

(67) Soe, C. M. M.; Stoumpos, C. C.; Kepenekian, M.; Traoré, B.; Tsai, H.; Nie, W.; Wang, B.; Katan, C.; Seshadri, R.; Mohite, A. D.; Even, J.; Marks, T. J.; Kanatzidis, M. G. New Type of 2D Perovskites with Alternating Cations in the Interlayer Space, $(C(NH_2)_3(CH_3NH_3)NPb_nI_{3n}^{+1}$: Structure, Properties, and Photovoltaic Performance. *J. Am. Chem. Soc.* **2017**, *139* (45), 16297–16309.

(68) Soe, C. M. M.; Nagabhushana, G. P.; Shivaramaiah, R.; Tsai, H.; Nie, W.; Blancon, J.-C.; Melkonyan, F.; Cao, D. H.; Traoré, B.; Pedesseau, L.; Kepenekian, M.; Katan, C.; Even, J.; Marks, T. J.; Navrotsky, A.; Mohite, A. D.; Stoumpos, C. C.; Kanatzidis, M. G. Structural and Thermodynamic Limits of Layer Thickness in 2D Halide Perovskites. *Proc. Natl. Acad. Sci.* **2019**, *116* (1), 58–66.

(69) Soe, C. M. M.; Nie, W.; Stoumpos, C. C.; Tsai, H.; Blancon, J.-C.; Liu, F.; Even, J.; Marks, T. J.; Mohite, A. D.; Kanatzidis, M. G. Understanding Film Formation Morphology and Orientation in High Member 2D Ruddlesden-Popper Perovskites for High-Efficiency Solar Cells. *Adv. Energy Mater.* **2017**, *1*, 1700979.

(70) Mao, L.; Kennard, R. M.; Traore, B.; Ke, W.; Katan, C.; Even, J.; Chabinyc, M. L.; Stoumpos, C. C.; Kanatzidis, M. G. Seven-Layered 2D Hybrid Lead Iodide Perovskites. *Chem* **2019**, *5* (10), 2593–2604.

(71) Proppe, A. H.; Quintero-Bermudez, R.; Tan, H.; Voznyy, O.; Kelley, S. O.; Sargent, E. H. Synthetic Control over Quantum Well Width Distribution and Carrier Migration in Low-Dimensional Perovskite Photovoltaics. *J. Am. Chem. Soc.* **2018**, *140* (8), 2890–2896.

(72) Wang, Z.; Lin, Q.; Chmiel, F. P.; Sakai, N.; Herz, L. M.; Snaith, H. J. Efficient Ambient-Air-Stable Solar Cells with 2D–3D Heterostructured Butylammonium-Caesium-Formamidinium Lead Halide Perovskites. *Nat. Energy* **2017**, *2* (9), 17135.

(73) Yoo, J. J.; Wieghold, S.; Sponseller, M. C.; Chua, M. R.; Bertram, S. N.; Hartono, N. T. P.; Tresback, J. S.; Hansen, E. C.; Correa-Baena, J. P.; Bulović, V.;

Buonassisi, T.; Shin, S. S.; Bawendi, M. G. An Interface Stabilized Perovskite Solar Cell with High Stabilized Efficiency and Low Voltage Loss. *Energy Environ. Sci.* **2019**, *12* (7), 2192–2199.

(74) Katan, C.; Mercier, N.; Even, J. Quantum and Dielectric Confinement Effects in Lower-Dimensional Hybrid Perovskite Semiconductors. *Chem. Rev.* **2019**, *119* (5), 3140–3192.

(75) Pedesseau, L.; Sapori, D.; Traore, B.; Robles, R.; Fang, H.; Loi, M. A.; Tsai, H.; Nie, W.; Blancon, J.; Neukirch, A.; Tretiak, S.; Mohite, A. D.; Katan, C.; Even, J.; Kepenekian, M. Advances and Promises of Layered Halide Hybrid Perovskite Semiconductors. *ACS Nano* **2016**, *10* (11), 9776–9786.

(76) Cao, D. H.; Stoumpos, C. C.; Farha, O. K.; Hupp, J. T.; Kanatzidis, M. G. 2D Homologous Perovskites as Light-Absorbing Materials for Solar Cell Applications. *J. Am. Chem. Soc.* **2015**, *137* (24), 7843–7850.

(77) Takagi, H.; Kunugita, H.; Ema, K. Influence of the Image Charge Effect on Excitonic Energy Structure in Organic-Inorganic Multiple Quantum Well Crystals. *Phys. Rev. B* **2013**, *87* (12), 125421.

(78) Smith, M. D.; Pedesseau, L.; Kepenekian, M.; Smith, I. C.; Katan, C.; Even, J.; Karunadasa, H. I. Decreasing the Electronic Confinement in Layered Perovskites through Intercalation. *Chem. Sci.* **2017**, *8* (3), 1960–1968.

(79) Ortiz-Cervantes, C.; Román-Román, P. I.; Vazquez-Chavez, J.; Hernández-Rodríguez, M.; Solis-Ibarra, D. Thousand-Fold Conductivity Increase in 2D Perovskites by Polydiacetylene Incorporation and Doping. *Angew. Chemie - Int. Ed.* **2018**, *57* (42), 13882–13886.

(80) Miyata, A.; Mitioglu, A.; Plochocka, P.; Portugall, O.; Wang, J. T.-W.; Stranks, S. D.; Snaith, H. J.; Nicholas, R. J. Direct Measurement of the Exciton Binding Energy and Effective Masses for Charge Carriers in Organic–inorganic Tri-Halide Perovskites. *Nat. Phys.* **2015**, *11* (7), 582–587.

(81) Even, J.; Pedesseau, L.; Katan, C. Understanding Quantum Confinement of Charge Carriers in Layered 2D Hybrid Perovskites. *ChemPhysChem* **2014**, *15* (17), 3733–3741.

(82) Blancon, J.-C.; Stier, A. V; Tsai, H.; Nie, W.; Stoumpos, C. C.; Traoré, B.; Pedesseau, L.; Kepenekian, M.; Katsutani, F.; Noe, G. T.; Kono, J.; Tretiak, S.; Crooker, S. A.; Katan, C.; Kanatzidis, M. G.; Crochet, J. J.; Even, J.; Mohite, A. D. Scaling Law for Excitons in 2D Perovskite Quantum Wells. *Nat. Commun.* **2018**,

9 (1), 2254.

(83) Lai, H.; Kan, B.; Liu, T.; Zheng, N.; Xie, Z.; Zhou, T.; Wan, X.; Zhang, X.; Liu, Y.; Chen, Y. Two-Dimensional Ruddlesden–Popper Perovskite with Nanorod-like Morphology for Solar Cells with Efficiency Exceeding 15%. *J. Am. Chem. Soc.* **2018**, *140* (37), 11639–11646.

(84) Ke, W.; Mao, L.; Stoumpos, C. C.; Hoffman, J.; Spanopoulos, I.; Mohite, A. D.; Kanatzidis, M. G. Compositional and Solvent Engineering in Dion-Jacobson 2D Perovskites Boosts Solar Cell Efficiency and Stability. *Adv. Energy Mater.* **2019**, 1803384.

(85) Fu, W.; Wang, J.; Zuo, L.; Gao, K.; Liu, F.; Ginger, D. S.; Jen, A. K. Y. Two-Dimensional Perovskite Solar Cells with 14.1% Power Conversion Efficiency and 0.68% External Radiative Efficiency. *ACS Energy Lett.* **2018**, *3* (9), 2086–2093.

(86) Chen, J.; Lian, X.; Zhang, Y.; Yang, W.; Li, J.; Qin, M.; Lu, X.; Wu, G.; Chen, H. Interfacial Engineering Enables High Efficiency with a High Open-Circuit Voltage above 1.23 V in 2D Perovskite Solar Cells. *J. Mater. Chem. A* **2018**, *6* (37), 18010–18017.

(87) Chen, Z.; Guo, Y.; Wertz, E.; Shi, J. Merits and Challenges of Ruddlesden-Popper Soft Halide Perovskites in Electro-Optics and Optoelectronics. *Adv. Mater.* **2019**, *31* (1), 1803514.

(88) Wang, H.; Fang, C.; Luo, H.; Li, D. Recent Progress of the Optoelectronic Properties of 2D Ruddlesden-Popper Perovskites. *J. Semicond.* **2019**, *40* (4), 041901.

(89) Ortiz-Cervantes, C.; Carmona-Monroy, P.; Solis-Ibarra, D. Two-Dimensional Halide Perovskites in Solar Cells: 2D or Not 2D? *ChemSusChem* **2019**, *12* (8), 1560–1575.

(90) Thrithamarassery Gangadharan, D.; Ma, D. Searching for Stability at Lower Dimensions: Current Trends and Future Prospects of Layered Perovskite Solar Cells. *Energy Environ. Sci.* **2019**, *12* (10), 2860–2889.

(91) Knutson, J. L.; Martin, J. D.; Mitzi, D. B. Tuning the Band Gap in Hybrid Tin Iodide Perovskite Semiconductors Using Structural Templating. *Inorg. Chem.* **2005**, *44* (13), 4699–4705.

(92) Katan, C.; Pedesseau, L.; Kepenekian, M.; Rolland, A.; Even, J. Interplay of Spin-Orbit Coupling and Lattice Distortion in Metal Substituted 3D Tri-Chloride Hybrid Perovskites. *J. Mater. Chem. A* **2015**, *3* (17), 9232–9240.

(93) Liu, G.; Kong, L.; Guo, P.; Stoumpos, C. C.; Hu, Q.; Liu, Z.; Cai, Z.; Gosztola, D. J.; Mao, H.; Kanatzidis, M. G.; Schaller, R. D. Two Regimes of Bandgap Red Shift and Partial Ambient Retention in Pressure-Treated Two-Dimensional Perovskites. *ACS Energy Lett.* **2017**, *2* (11), 2518–2524.

(94) Chen, M.; Ju, M.-G.; Hu, M.; Dai, Z.; Hu, Y.; Rong, Y.; Han, H.; Zeng, X. C.; Zhou, Y.; Padture, N. P. Lead-Free Dion–Jacobson Tin Halide Perovskites for Photovoltaics. *ACS Energy Lett.* **2019**, *4* (1), 276–277.

(95) Safdari, M.; Svensson, P. H.; Hoang, M. T.; Oh, I.; Kloo, L.; Gardner, J. M. Layered 2D Alkyldiammonium Lead Iodide Perovskites: Synthesis, Characterization, and Use in Solar Cells. *J. Mater. Chem. A* **2016**, *4* (40), 15638–15646.

(96) Safdari, M.; Phuyal, D.; Philippe, B.; Svensson, P. H.; Butorin, S. M.; Kvashnina, K. O.; Rensmo, H.; Kloo, L.; Gardner, J. M. Impact of Synthetic Routes on the Structural and Physical Properties of Butyl-1,4-Diammonium Lead Iodide Semiconductors. *J. Mater. Chem. A* **2017**, *5* (23), 11730–11738.

(97) Li, Y.; Milić, J. V.; Ummadisingu, A.; Seo, J.; Im, J.; Kim, H.; Liu, Y.; Dar, M. I.; Zakeeruddin, S. M.; Wang, P.; Hagfeldt, A.; Grätzel, M. Bifunctional Organic Spacers for Formamidinium-Based Hybrid Dion–Jacobson Two-Dimensional Perovskite Solar Cells. *Nano Lett.* **2019**, *19* (1), 150–157.

(98) Diau, E. W.; Jokar, E.; Rameez, M. Strategies To Improve Performance and Stability for Tin-Based Perovskite Solar Cells. *ACS Energy Lett.* **2019**, 1930–1937.

(99) Stoumpos, C. C.; Malliakas, C. D.; Kanatzidis, M. G. Organic Tin and Lead Iodide Perovskites with Organic Cations : Unique Semiconductors, with Phase Transitions and Near-Infrared Photoluminescent Properties. *Inorg. Chem.* **2013**, *52* (15), 9019–9038.

(100) Ke, W.; Stoumpos, C. C.; Kanatzidis, M. G. "Unleaded" Perovskites: Status Quo and Future Prospects of Tin-Based Perovskite Solar Cells. *Adv. Mater.* **2018**, 1803230.

(101) Wang, F.; Jiang, X.; Chen, H.; Shang, Y.; Liu, H.; Wei, J.; Zhou, W.; He, H.; Liu, W.; Ning, Z. 2D-Quasi-2D-3D Hierarchy Structure for Tin Perovskite Solar Cells with Enhanced Efficiency and Stability. *Joule* **2018**, *2* (12), 2732–2743.

(102) Lemmerer, A.; Billing, D. G. Lead Halide Inorganic–organic Hybrids Incorporating Diammonium Cations. *CrystEngComm* **2012**, *14* (6), 1954.

(103) Sourisseau, S.; Louvain, N.; Bi, W.; Mercier, N.; Rondeau, D.; Boucher, F.; Buzaré,

J.-Y.; Legein, C. Reduced Band Gap Hybrid Perovskites Resulting from Combined Hydrogen and Halogen Bonding at the Organic−Inorganic Interface. *Chem. Mater.* **2007**, *19* (3), 600–607.

(104) Blancon, J.-C.; Tsai, H.; Nie, W.; Stoumpos, C. C.; Pedesseau, L.; Katan, C.; Kepenekian, M.; Soe, C. M. M.; Appavoo, K.; Sfeir, M. Y.; Tretiak, S.; Ajayan, P. M.; Kanatzidis, M. G.; Even, J.; Crochet, J. J.; Mohite, A. D. Extremely Efficient Internal Exciton Dissociation through Edge States in Layered 2D Perovskites. *Science.* **2017**, *355* (6331), 1288–1292.

(105) Zhang, X.; Wu, G.; Yang, S.; Fu, W.; Zhang, Z.; Chen, C.; Liu, W.; Yan, J.; Yang, W.; Chen, H. Vertically Oriented 2D Layered Perovskite Solar Cells with Enhanced Efficiency and Good Stability. *Small* **2017**, *13* (33), 1700611.

(106) Yan, J.; Fu, W.; Zhang, X.; Chen, J.; Yang, W.; Qiu, W.; Wu, G.; Liu, F.; Heremans, P.; Chen, H. Highly Oriented Two-Dimensional Formamidinium Lead Iodide Perovskites with a Small Bandgap of 1.51 eV. *Mater. Chem. Front.* **2018**, *2* (1), 121–128.

(107) Gottesman, R.; Lopez-Varo, P.; Gouda, L.; Jimenez-Tejada, J. A.; Hu, J.; Tirosh, S.; Zaban, A.; Bisquert, J. Dynamic Phenomena at Perovskite/Electron-Selective Contact Interface as Interpreted from Photovoltage Decays. *Chem* **2016**, *1* (5), 776–789.

(108) Kepenekian, M.; Traore, B.; Blancon, J.-C.; Pedesseau, L.; Tsai, H.; Nie, W.; Stoumpos, C. C.; Kanatzidis, M. G.; Even, J.; Mohite, A. D.; Tretiak, S.; Katan, C. Concept of Lattice Mismatch and Emergence of Surface States in Two-Dimensional Hybrid Perovskite Quantum Wells. *Nano Lett.* **2018**, *18* (9), 5603–5609.

Three quotes:

(1): ¨These significant developments in the field of Dion-Jacobson phase perovskites demonstrate its incredible potential as semiconducting active layers aiming to fabricate efficient yet long-term stable PSCs.¨

(2): ¨The competitive advantages of Dion-Jacobson perovskites over RP counterparts are outlined, such as improved stability and electrical properties.¨

(3): ¨ A possible approach to improve the long-term, operational stability of Dion-Jacobson layered PSCs under harsh conditions can be the replacement of the A-site organic cation (MA^+, FA^+) with inorganic cation such as Cs^+, Rb^+ or their mixed alloy.¨

TOC

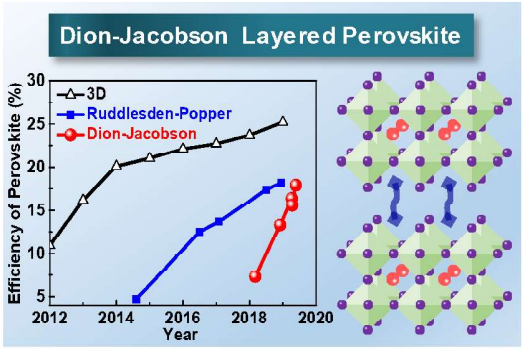

A time scale showing the fast evolution of DJ perovskite reaching high PCE.